On the Effect of Manipulating Large Scale Motions in a Boundary Layer

Akshit Jariwala *, Alexandros Tsolovikos †, Saikishan Suryanarayanan ‡, Efstathios Bakolas §, and David Goldstein ¶

The University of Texas at Austin, Austin, Texas 78712-1085

Large Scale Motions (LSMs) are coherent structures that naturally occur in a turbulent boundary layer. These vortical structures carry a significant portion of the turbulent kinetic energy (TKE) and have the potential to actively change the dynamics of the boundary layer. We, therefore, argue that by systematically manipulating these structures, one can leverage their potential for technological benefits, such as separation control, drag reduction, or mixing enhancement. In our previous work, it was shown that steering vortical structures in a laminar boundary layer increases mixing near the wall (Tsolovikos et al. AIAA J.,59(10), 4057, 2021). In our present work, we extend this analysis to synthetically-generated LSMs that resemble naturally occurring LSMs consisting of hairpin packets. The synthetic LSMs are generated within a zero pressure gradient laminar boundary layer using a carefully tuned, time-dependent external force field. The synthetic LSMs are then steered toward the wall by a secondary force field that creates a localized downwash region. The evolution of the uncontrolled and controlled LSMs is characterized in terms of their spatiotemporally developing momentum, TKE, detailed structures, and other parameters relevant to the re-energization of the near-wall flow. The results demonstrate that steering synthetically generated vortical structures that resemble LSMs toward the wall has the expected effect of increasing near wall vorticity and wall shear stress.

I. Nomenclature

 δ = Nominal boundary layer thickness based on $0.99U_{\infty}$

dt = Time step

 U_{∞} = Free stream velocity

u= Velocity vector with 3 components (u_x, u_u, u_z) ω = Vorticity vector with 3 components (ω_x, ω_y, ω_z)

 ν = Kinematic viscosity

 Re_{δ} = Reynolds number based on the boundary layer thickness δ and the free-stream velocity

 τ_w = Wall shear stress β = Decay factor

R = Radius of the core region

 L_x = Length of the domain in streamwise direction L_y = Length of the domain in wall-normal direction L_z = Length of the domain in spanwise direction

 \mathbf{g}^{LSM} = LSM force field center \mathbf{g}^{Jet} = Jet force field center

 x_c = X coordinate of the centroid of the perturbation y_c = Y coordinate of the centroid of the perturbation z_c = Z coordinate of the centroid of the perturbation

^{*}Graduate Student, Department of Aerospace Engineering and Engineering Mechanics, The University of Texas at Austin, Student Member.

[†]Graduate Student, Department of Aerospace Engineering and Engineering Mechanics, The University of Texas at Austin, Student Member.

^{*}Research Associate, Department of Aerospace Engineering and Engineering Mechanics, The University of Texas at Austin, Member.

[§] Associate Professor, Department of Aerospace Engineering and Engineering Mechanics, The University of Texas at Austin, Senior Member.

[¶]Professor, Department of Aerospace Engineering and Engineering Mechanics, The University of Texas at Austin, Associate Fellow.

II. Introduction

It is understood that wall-bounded turbulent flows largely consist of coherent structures including – the so-called large scale motions (LSMs) – with significant turbulent kinetic energy [1]. These structures persist over long periods within the flow and they exhibit significant temporal and spatial correlation [2]. These structures may be controlled in a manner such that their energy potential can be used to achieve performance gains, such as mixing enhancement or separation delay. These LSMs have a size and thickness in the order of the boundary layer thickness δ , and can be understood as a series of hairpin vortex packets [3], [4],[5].

Ideal hairpin vortices are a type of vortex structures consisting of a rotating head with its axis, oriented in the span-wise direction, with two adjacent legs in the upstream and wall-normal directions [6]. Hairpin vortices can be viewed as the building blocks of LSMs in turbulent boundary layers, where they coherently align into structures that are long in the streamwise direction [7]. Furthermore, using spectral analysis, [8] found that the spectral peak of LSMs matched that of a hairpin packet (a series of hairpin vortices aligned in the stream-wise direction), lending to the belief that LSMs are indeed composed of a concatenation of hairpin vortices. The formation mechanism for hairpin vortices is believed to be the alignment of the low momentum zones located underneath the heads of individual hairpin vortices [9]. This mechanism is central in our approach to producing these structures synthetically within the laminar boundary layer for further examination.

For our needs, it is necessary to examine the shapes of these structures within the turbulent boundary layer. Structures with a length less than 0.1δ can be identified as small-scale turbulent structures, such as eddies or hairpins [5]. In [10], the authors also suggested that another critical length to distinguish between an LSM and VLSM (very large-scale motion) is about 2.9δ , with VLSMs having streamwise sizes more than 3δ . These lengths appear to scale even to very high Reynolds numbers characteristic of atmospheric boundary layers [9]. The LSMs and VLSMs found in the logarithmic or outer regions of a turbulent boundary layer typically consist of small-scale structures, such as hairpin vortices and clusters of hairpins, and contain about half of the turbulent kinetic energy and more than half of the Reynolds shear stress [1]. Similarly, in turbulent channel flows, as the Reynolds number increases, more kinetic energy is carried by VLSMs than by LSMs [11].

One can think of these LSMs as a uniform sequence of hairpins that may be manipulated to re-energize the boundary layer, reduce drag, or enhance mixing. In this work, initial efforts are shown on how to generate hairpins packets in a laminar boundary layer flow to create a synthetic LSM that approximates a naturally-occurring LSM. In [6], the authors observed that applying short and intense pulses gave the best results for creating a single leading hairpin, but secondary hairpins were created shortly after the forcing ceased, leading to a turbulent spot further downstream. Similarly, in [12], the authors created a straight vortex tube in a laminar boundary layer flow upon which hairpins grew.

In this work, we aim to generate and move synthetically-generated LSMs toward the wall and study the effect of such a control scheme on the near-wall statistics. We present details on how to create these hairpins synthetically in a laminar flow. Preliminary results of moving synthetic LSMs toward the wall using a downwash-inducing jet force field are obtained to see how the energy potential of LSMs can be harnessed by steering them toward the wall in order to increase near-wall momentum and potentially delay flow separation. We have chosen to carry out this study in the laminar boundary layer to study the interaction between the synthetic LSMs and the jet. Turbulent boundary layer direct numerical simulations are computationally expensive and it is difficult to reproduce the results. Furthermore, within the turbulent boundary layer, these hairpins might decay rapidly and one might need to do ensemble averaging to notice any spatiotemporal evolution. We argue that in order to control the LSMs in the turbulent layer flow, one must understand the effect of controlling LSMs in the laminar boundary layer. The present study is a step towards the towards the turbulent boundary layer which will be performed in the near future.

To synthetically generate these LSM in a laminar boundary layer, a forcing is used necessary to perturb the flow. In a direct numerical simulation (DNS), this can be done by an external force field. The shape, magnitude, and temporal distribution of such a force field play a critical role in generating realistic LSMs. We perform a parametric study to find the optimal parameters for a given Re_{δ} . The Direct Numerical Simulation presented here are performed using the open source spectral element solver (NEK5000 [13]). The details of the numerical setup are presented in Section III. As these needed forcing parameters are sensitive to flow parameters, such as the Reynolds number, boundary layer thickness, and free stream velocity, a laminar condition provides a stable flow condition throughout the domain and a better understanding of the results of forcing.

Although there are many ways one could use an external force field to generate a series of hairpin vortices, the one we chose to use is described in the Section III. A detailed parametric study has been carried out to determine the optimal forcing parameters that generate synthetic LSMs that are ideal for the present study (Section IV).

To quantify the forcing used to generate the synthetic LSMs, we calculate the impulse of the forcing, which is the

time and volumetric integral of the force field in the domain. A set of metrics is used to quantify the effect of LSMs on the flow with and without steering. First, the average wall shear stress is measured downstream of the perturbation. Second, the vorticity fluctuation root mean square (RMS) wall-normal distribution is computed at different streamwise locations. For both metrics, we study three different scenarios: 1) the effect of hairpins only on near-wall vorticity and shear stress, 2) the effect of hairpins combined with steering using jet actuation to bring them close to a wall, and, lastly, 3) the only the effects of jet actuation to measure the relative performance.

Manipulation of these LSMs is done by an actuator modeled as a downwash-inducing jet force field, explained in the Section III. The schematic of the computational setup is shown in Fig. 1, where the jet is shown to bring a series of hairpin vortices closer to the wall by the induced downwash. The decision of when to actuate (turn the actuator on and off) is determined by examining the location of the hairpins at a given time and setting the actuator parameters in the consequent simulation for the given location of actuator \mathbf{g}^{Jet} .

III. Numerical Setup

A. Computational Setup

To generate synthetic LSMs and test our control scheme, we employ high fidelity direct numerical simulations using NEK5000 [13] a widely used and highly scalable spectral element code [14, 15]. Zero-pressure-gradient laminar boundary layer simulations are performed with a Blasius velocity profile a the inlet, no-slip boundary condition at the wall, periodic boundary conditions in the spanwise direction, and an outflow boundary condition ($[-pI + \nu(\nabla \mathbf{u})] \cdot \mathbf{n} = 0$) at the top and at the outlet are applied. The inlet Blasius profile at a specific boundary layer thickness δ and the initial condition is the Blasius velocity profile over the entire length of the domain, scaled according to each x location. Two separate external force fields are used to first generate the synthetic LSMs (Subsection III.B) and then to actuate upon them (Subsection III.C). The setup of the computational domain is illustrated in the Fig. 1.

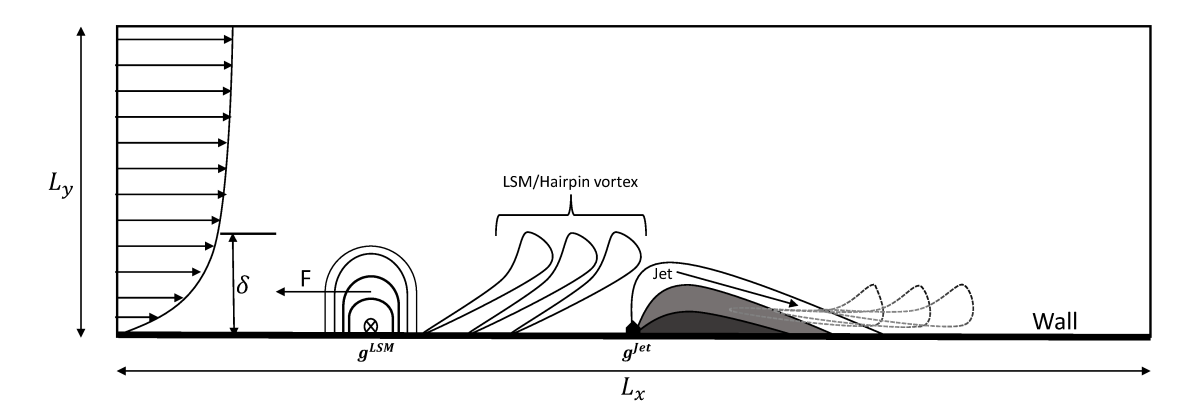


Fig. 1 DNS setup of the computational domain (spanwise normal slice at the center of the domain).

For the parametric study performed in the Section IV, the boundary layer thickness is chosen to be $\delta_{99} = 0.3$ at the inlet and the Reynolds number based on the boundary layer thickness is set to $Re_{\delta} = 1000$. The size of the computational domain is $30\delta \times 3\delta \times 6\delta$ in the streamwise, wall-normal, and spanwise directions, respectively. The number of elements in each direction is $80 \times 16 \times 16$, the order of each element is 7, and the distribution of elements in the wall-normal direction is scaled by a hyperbolic tangent (with finer discretization near the wall), while the distribution in the streamwise and spanwise directions is uniform. The time step for the DNS is dt = 0.0025 (nondimensional).

B. Generating Synthetic LSMs

The force field to generate the LSMs is modeled as a tanh-smooth distribution in space with a fixed centroid location $\mathbf{g}^{LSM} = [x_c^{LSM}, y_c^{LSM}, z_c^{LSM}]$, forcing upstream of the flow (in negative x direction). The external force is described as

$$\mathbf{f}^{LSM}(x, y, z, A^{LSM}) = \left[f_x^{LSM}(x, y, z, A^{LSM}), 0, 0 \right] \tag{1}$$

where

$$\begin{split} f_x^{LSM}(x,y,z,A^{LSM}) &= -A^{LSM} \frac{1}{2} [1 + \tanh \left(\beta_x (R_x - |x - x_c^{LSM}|)\right)] \\ &\times \frac{1}{2} [1 + \tanh \left(\beta_y (R_y - |y - y_c^{LSM}|)\right)] \\ &\times \frac{1}{2} [1 + \tanh \left(\beta_z (R_z - |z - z_c^{LSM}|)\right)] \end{split} \tag{2}$$

In the above equations, $A^{LSM} \ge 0$ is the time-varying amplitude that describes the temporal evolution of the force field, $\beta_x, \beta_y, \beta_z > 0$ is the decay factor in each direction, and $R_x, R_y, R_z \in [0, 1]$ is the radius of the core region in each direction. All three of these parameters contribute significantly to how the force field is distributed in space and time. A parametric study of these parameters is carried out to better understand the effect of the different variations on the resulting hairpins further downstream. The parametric study is discussed in Subsection IV.B.

In order to produce strong impulses by forcing upstream that can create a low momentum streak on which hairpin vortices can develop, the temporal variation of the amplitude A^{LSM} of the LSM force field can be controlled in various ways. For example, one can simply use the rectified sinusoidal wave function $(\max(\text{sine}(\cdot), 0))$ to vary the amplitude A^{LSM} in time. Different time-varying actuation schemes that are tested for the parametric study are discussed in Subsection IV.A. Here, one thing to notice is that this actuation of forcing is not periodic but rather transient, lasting only for a finite amount of time. It was noticed that prolonged forcing eventually evolved into a local turbulent spot which was undesirable. Also, our goal was to emulate a finite sized LSM.

C. Actuator Force Field

Once the synthetic LSMs are generated, we target them and move them toward the wall using a secondary force field located downstream of the LSM-generating force field. This secondary force field acts as the actuator in our flow control setting, turning on and off on demand and generating a downwash strong enough to move the LSMs closer to the wall, but not too strong to cause boundary layer instabilities. The actuator force field is an external force field centered at $\mathbf{g}^{Jet} = [x_c^{Jet}, y_c^{Jet}, z_c^{Jet}]$ and defined as

$$\mathbf{f}^{Jet}(x, y, z, A^{Jet}) = \left[f_x^{Jet}(x, y, z, A^{Jet}), f_y^{Jet}(x, y, z, A^{Jet}), 0 \right], \tag{3}$$

where

$$f_x^{Jet}(x, y, z, A^{Jet}) = -f_y(x, y, z, A^{Jet}) = \frac{1}{2} A^{Jet} \frac{x - x_c^{Jet}}{\alpha_x} \exp\left(1 - \frac{x - x_c^{Jet}}{\alpha_x}\right) \exp\left(-\frac{1}{2} \frac{(y - y_c^{Jet})^2}{\alpha_y^2} - \frac{1}{2} \frac{(z - z_c^{Jet})^2}{\alpha_z^2}\right). \tag{4}$$

The spatial distribution of the force field follows a gamma distribution with shape parameter 2 in the streamwise direction and a Gaussian distribution in the wall-normal and spanwise directions. The magnitude of the force field is controlled by a scalar *control input* $A^{Jet} \in [0,1]$. This force field effectively accelerates the near-wall flow and induces a downwash when $A^{Jet} \neq 0$. The parameters of the distribution are chosen to be $\alpha_x = 0.5$, $\alpha_x = 0.25$, $\alpha_x = 0.25$, such that the induced downwash will roughly cover the entire height and span of the generated LSMs. The choice of a gamma distribution for the downwash-inducing force field is motivated by the effect that dielectric barrier discharge plasma actuators have on the near-wall flow [16].

IV. Parametric Study

For the parametric study of generating synthetic LSMs, a reference set of parameters is empirically chosen for the baseline case and the effects of varying the main parameters of the force field around that baseline is studied. The parameters of the baseline case are listed in Table 1

Figure 2a shows the baseline spatial distribution of the forcing profile used to generate the LSMs. The force field is higher at the centroid and decreases away from it. The distribution in all directions is a smooth tanh function. Naturally-occurring hairpins in a boundary layer may form on and ride on top of a low-speed streak. Hence, the strong upstream force in the core region near the wall should create this low-speed fluid within the boundary layer, with vortical

| Spatial Parameter Values | | |
|---------------------------|---|------|
| β_x | Decay factor in X-dir. | 10 |
| β_y | Decay factor in Y-Dir. | 10 |
| β_z | Decay factor in Z-Dir. | 10 |
| R_x | Radius of the core region in X-Dir. | 0.2 |
| R_y | Radius of the core region in Y-Dir. | 0.2 |
| R_z | Radius of the core region in Z-Dir. | 0.2 |
| Temporal Parameter Values | | |
| A_1 | Max. Amplitude of the base forcing | 0.5 |
| A_2 | Max. Amplitude of the actuation top of the base | 0.5 |
| t_1 | Total number of iteration for $\mathbf{f}^L SM$ | 2400 |
| t_2 | No. of iterations for which $A_1 < A^{LSM} < A_1 + A_2$ | 200 |
| <i>t</i> ₃ | No. of iteration between consecutive pulses for which $0 \le A^{LSM} \le A_1$ | 500 |

Table 1 Parameters used for the baseline synthetic LSM generating force field

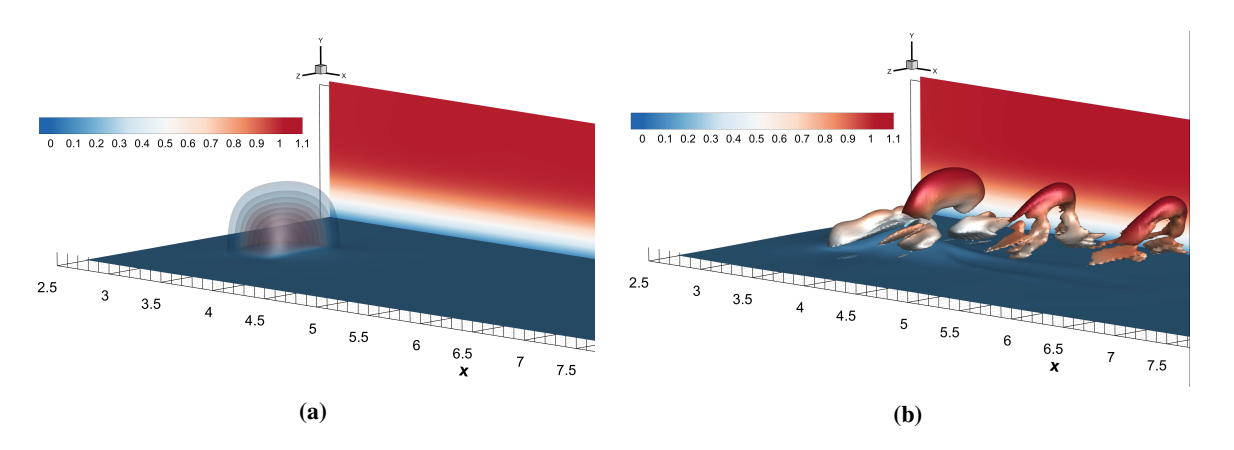


Fig. 2 (a) Spatial volumetric forcing profile located at g^{LSM} with the side wall colored by the streamwise velocity. (b) Isosurface of λ_2 of the resulting hairpin vortices colored by the streamwise velocity.

structures riding on top of low speed region, as shown in Fig. 2b. It is also evident that forcing upstream does create vortical structure in the downstream region as shown in Fig. 2b.

In Subsection IV.A, different amplitude signals A^{LSM} are considered, as shown in Fig. 3, while in Subsection IV.B, all six of the shape-affecting parameters are varied in order to understand the effect of each one individually.

To ensure that the comparisons are fair, each parameter set of the force field is chosen such that the impulse of the external force field,

$$I = \iint_{V,t} \mathbf{f}^{LSM} \, dV \, dt \tag{5}$$

is the same in all cases.

A. Temporal Distribution Study

We test three different temporal distributions of the amplitude A^{LSM} of the LSM-generating force field, as shown in Fig. 3. The first case (Fig. 3a) is a (half) sinusoidal distribution with two characteristic amplitudes: the amplitude A_1 of a pedestal forcing and the secondary amplitude A_2 of the rectified sinusoidal pulse. The second case (Fig. 3b) is a rectified sine wave with no base forcing. The third case (Fig. 3c) is a square wave.

For each of the above distributions, we run different cases with varying temporal parameters to control the evolution

of the hairpin packets, such that their size and shape matches the size and shape of the expected naturally-occurring hairpin packets [11],[10]. It is desired to have 3-4 hairpins in a stretch of $2-3\delta$ in the streamwise direction. Our studies have shown that pulsing too vigorously and with little time between consecutive pulses eventually or perhaps quickly leads to a turbulent spot. The reason behind this transition is further discussed in Section V. Creating a turbulent spot defeats the purpose of this study, since it rapidly grows in space and does not lead to a realistic representation of an LSM that we can isolate, study, and manipulate. Carefully tuning the parameters is crucial to get isolated and stable hairpins as they further evolve in the domain.

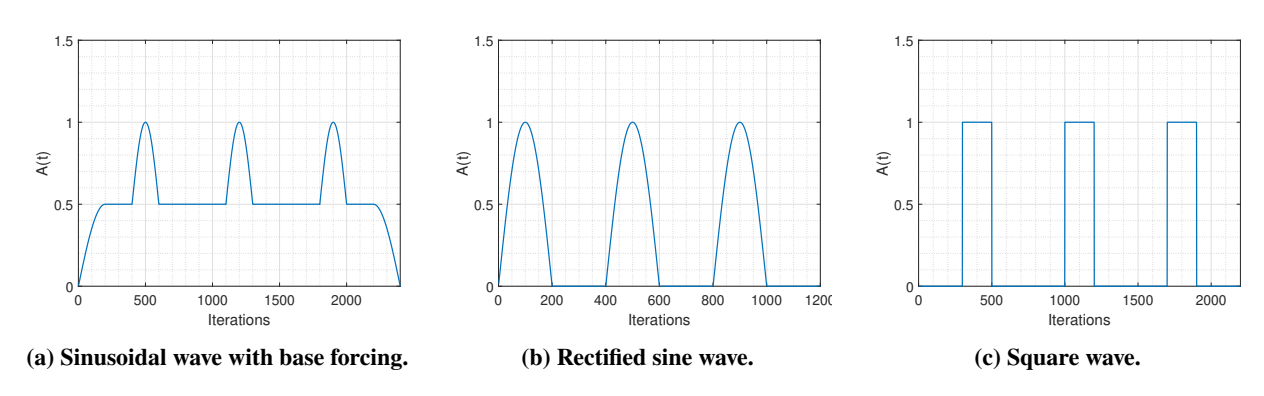


Fig. 3 Different temporal distributions of the forcing.

Having performed simulations using the types of time-varying forcing profile in Fig. 3c, it was found that the sudden introduction of forcing using the square wave function resulted in the creation of small scale vortical structures. These small scale structures hindered the ability to obtain a clean series of hairpins and appear to result in the latter hairpins eventually evolving into a turbulent spot. To alleviate these persistent smaller-scale structures, the forcing profile needs to feature a smoother increase to the maximum value. Having examined several options, it was determined that gradually increasing the forcing amplitude in a sinusoidal way is preferred.

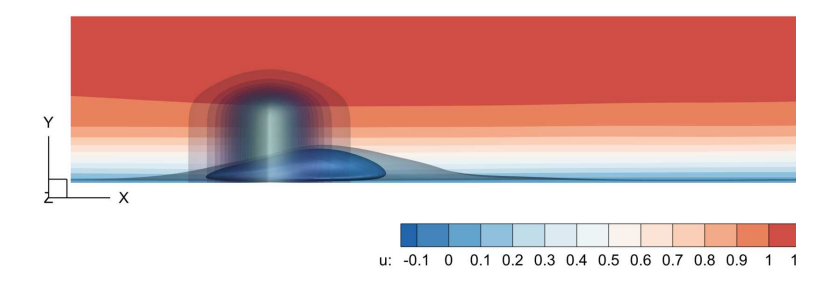


Fig. 4 Separation bubble created by the constant upstream forcing colored by blue iso-surface of stream-wise velocity

Similarly, the profile shown in Fig. 3a also led to the creation of a local separation bubble that eventually broke into small scale structures.

The separation bubble is believed to be created by the constant portion of the upstream forcing and it breaks up after the body force is removed. Figure 4 shows the streamwise velocity iso-surface close to the wall for the Fig. 3a. Within this region, the velocity is negative as the flow near the wall is already very slow and upstream forcing locally reduces the momentum. For the reasons mentioned above, we have decided to use the rectified sine wave distribution of Fig. 3b for the rest of the study, since the effect illustrated in Fig. 4 easily occurs with the forcing amplitude of Fig. 3a.

B. Spatial Distribution Study

It is seen in Fig. 2b that we can create a series of clean hairpin vortices within the laminar boundary layer, which can then be treated as LSMs. Thorough refinement of the free variables is needed as undesired structures still follow

these hairpins. A parametric study is carried out, where each of the spatial parameters listed in Table 1 is varied in order to understand its effect on the generated hairpins.

As illustrated in Fig. 5, increasing the decay factors β_x , β_y , β_z squeezes the force distribution in the respective direction, meaning the force decays a lot faster in that particular direction. While keeping the impulse value equal to the base reference case calculated using the Eq. (5). This parameter is mainly used to control the force distribution within the core region.

Similarly, increasing and decreasing the radii R_x , R_y , R_z of the core region increases and decreases, respectively, the length, height, and width of the force field. This parameter has direct influence on the shape of the hairpins. The radius of the core region can affect how wide the hairpins are further downstream. As indicated in [17], these LSMs have a spanwise width in the order of the boundary layer thickness δ . In particular, increasing R_z increases the overall width in the spanwise direction of the spatial distribution, as seen in Fig. 5f, and thus it affects the width of the LSMs. Controlling this parameter can therefore help us achieve our goal of generating packets of hairpins that are close to δ wide.

We were able to create a series of vortical structure that closely resemble hairpin vortices, but are not quite as stable and clean as we would like them to be (Fig. 6). During the parametric study, it was realized that the strong upstream forcing in the core region creates a separation bubble as shown in Fig. 4, which eventually breaks up, creating a turbulent spot. The spot is visible in Fig.6 at the center of the force field. This effect was inevitable even with the rectified sinusoidal wave amplitude (Fig. 3b).

To avoid this break up of the separation bubble caused by the upstream forcing, the force field was modified to remove the strong forcing from the core region. This is done by setting the force to zero when it exceeds a magnitude of f_{max} creating more of a donut like forcing volume. Because of the reduced amount of forcing, the separation bubble does not evolve as much as before. Even if, the impulse value is kept the same. This has been done by changing the values of β and R. After numerous trials and errors, we were able to achieve the results shown in Fig. 7. The small-scale features seen close to the wall trailing behind the hairpins eventually decay due to high shear within the boundary layer and do not evolve into a turbulent spot further downstream.

V. Results of Applying Control Jet

We expect that manipulating the synthetic LSMs and pushing them toward the wall will increase wall shear stress and near-wall mixing, similar to [18], where random vortical disturbances were targeted instead of trains of hairpin vortices. Many of the free parameters for the problem, such as those defining the shape of the LSM-generating force field, are empirically chosen, following the parametric study discussed above to generate qualitatively satisfactory synthetic LSMs, Fig. 7. The frequency of the pulsing, namely the temporal parameters t_2 and t_3 , are also chosen in a way such that each hairpin has enough time to fully develop and not create a turbulent spot as it moves downstream.

Our goal is to increase near-wall mixing and wall shear stress by creating a downwash using the actuator force field (jet) of Subsection III.C that will push the synthetic LSMs closer to the wall. Of course, both the synthetic LSMs and the jet affect the near-wall flow properties of the flow on their own. However, by combining the two and bringing the LSMs closer to the wall, we hope to achieve enhanced mixing, more than simply their additive contributions. Two metrics are used to study the flow near the wall: the wall shear stress τ_w and the root mean square (RMS) of the vorticity fluctuations ω'_{rms} , which are defined as

$$\omega_{rms}(x_i, y) = \sqrt{\frac{1}{T \times L_z} \int_{t=0}^{t=T} \int_{z=0}^{z=L_z} (\omega_x')^2 + (\omega_y')^2 + (\omega_z')^2 dz dt}$$
 (6)

$$\tau_w(t) = \frac{1}{A_{xz}} \int_{x=x_\alpha}^{x=L_x} \int_{z=0}^{z=L_z} \frac{\partial u}{\partial y} \Big|_{w} dz dx$$
 (7)

To quantify the effect of this actuation scheme, we examine the wall-shear stress (Fig. 8) and the vorticity fluctuation RMS Fig. (9). In each figure, we compare three different cases: 1) the LSM only case, where there is no actuation (no jet downwash), 2) the jet only case, to compare the effect of the added vorticity and shear due to the jet itself, and 3) the LSM plus jet case, where the LSM moves closer the wall thanks to the downwash induced by the jet.

We have used the wall shear stress averaged over the area, where the area is entire downstream region starting from the jet location (\mathbf{g}^{Jet}) to the end of the domain. Figure 8 clearly indicates an increase of τ_w when targeting the LSMs (LSM + Jet) compared to the other two cases. This trend is repeated even when the strength of the jet A^{jet} is reduced (thus creating a weaker downwash). Although the maximum τ_w for the case of the LSM + Jet is less with the weaker jet

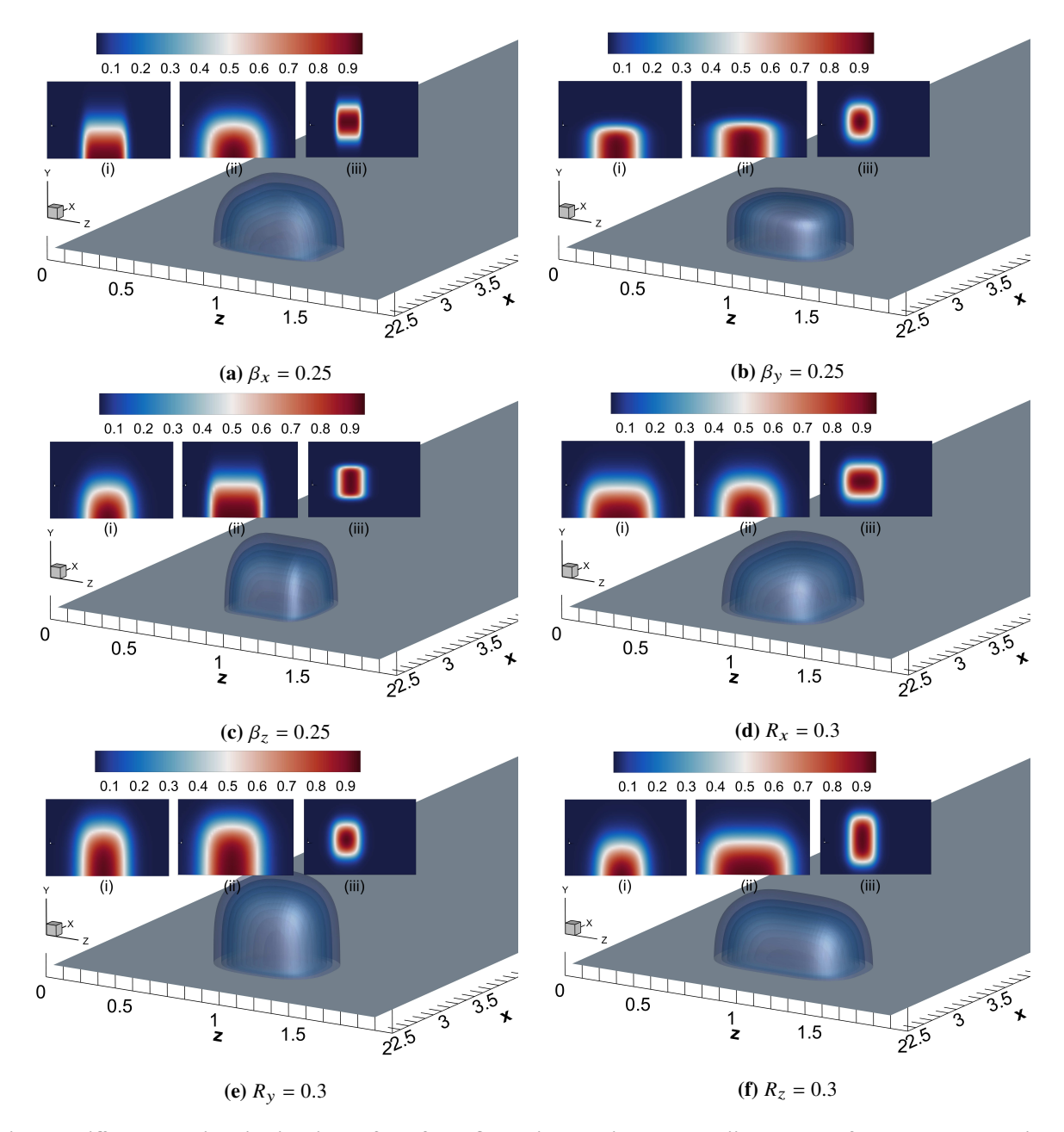


Fig. 5 Different spatial distributions of the force field with varying core radii and decay factors. The three inset figures in each main figure show (i) x-y, (ii) z-y, and (iii) x-z slices of the distribution through the center of the force field \mathbf{g}^{LSM} .

of $A^{jet} = 0.5$, it is interesting to notice that the underline gain is higher than that of the strong jet $(A^{jet} = 1)$. Also, the ω_{rms} with the weaker jet (Fig. 9b) is greater compared to the case where the jet actuation is strong. This is observed at x = 6 and x = 7 closer to the jet location. This suggests that the vorticity field associated with the LSMs has moved closer to the wall, leading to an increase in the near wall vortical activity downstream of the actuator. In the case of strong actuation, a similar observation is made, although less noticeable due to the higher strength of the jet. These results directly corroborate the results presented in [18], where random vortical structures were introduced in the flow to test the model predictive algorithms for the jet actuation scheme.

In both cases ($A^{jet} = 1$ and $A^{jet} = 0.5$), the ω_{rms} is much higher close to wall at x = 5 and lower further away from the wall. However, as we move further downstream, the vorticity fluctuations spread away from the wall.

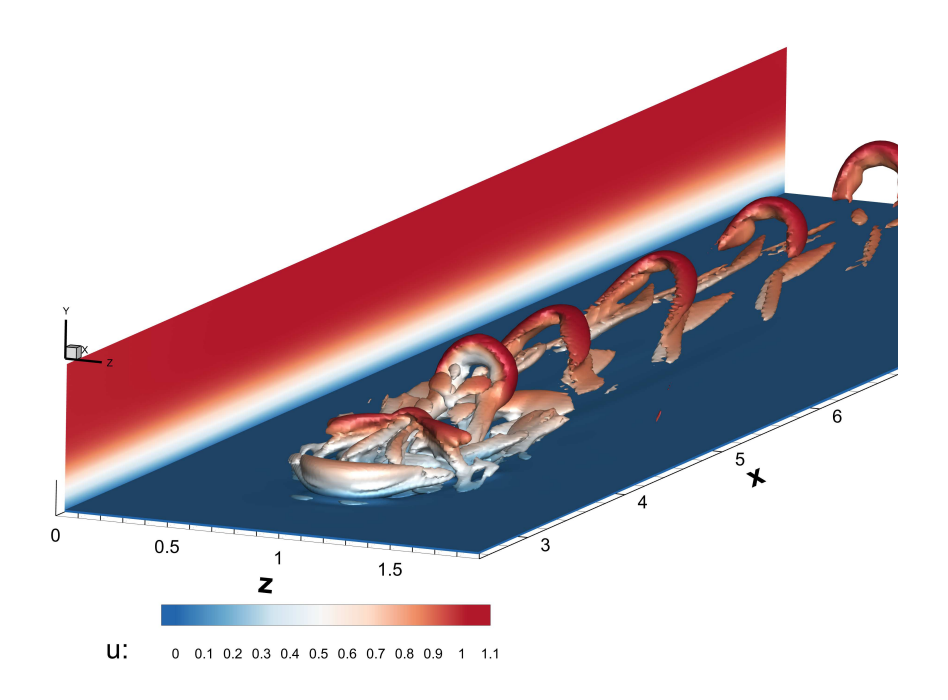


Fig. 6 Evolution of the series of vortical structure with clear indication of turbulent spot at the forcing location.

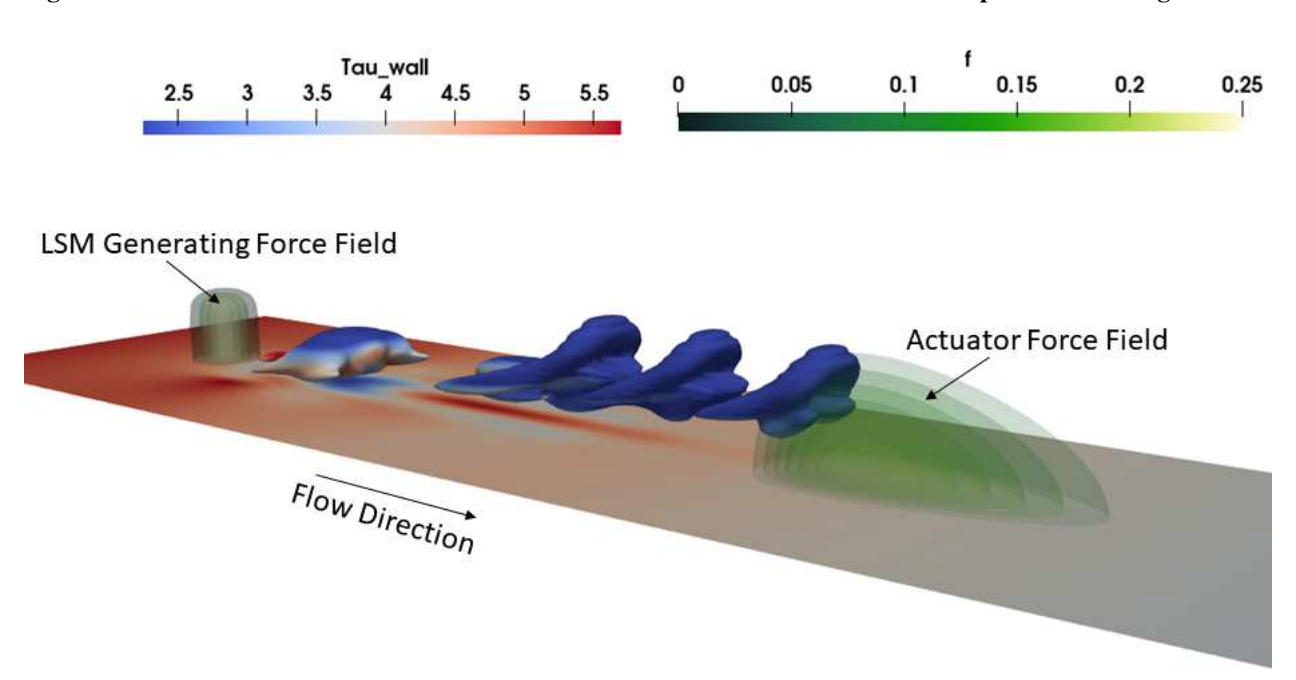


Fig. 7 Iso-surfaces of the Q criterion of a train of hairpins colored by the shear stress. Note that the wall is also colored by the (wall) shear stress and force field iso-surfaces are colored by it's magnitude

For the purposes of this study, the decision of when to turn the jet on and off is done by observation. We know when the generated LSMs will approach the actuator force field and its induced downwash region and, therefore, we can time when to turn the actuation on and off. A more principled (and automated) way of controlling the actuator for targeting LSMs was presented in [18].

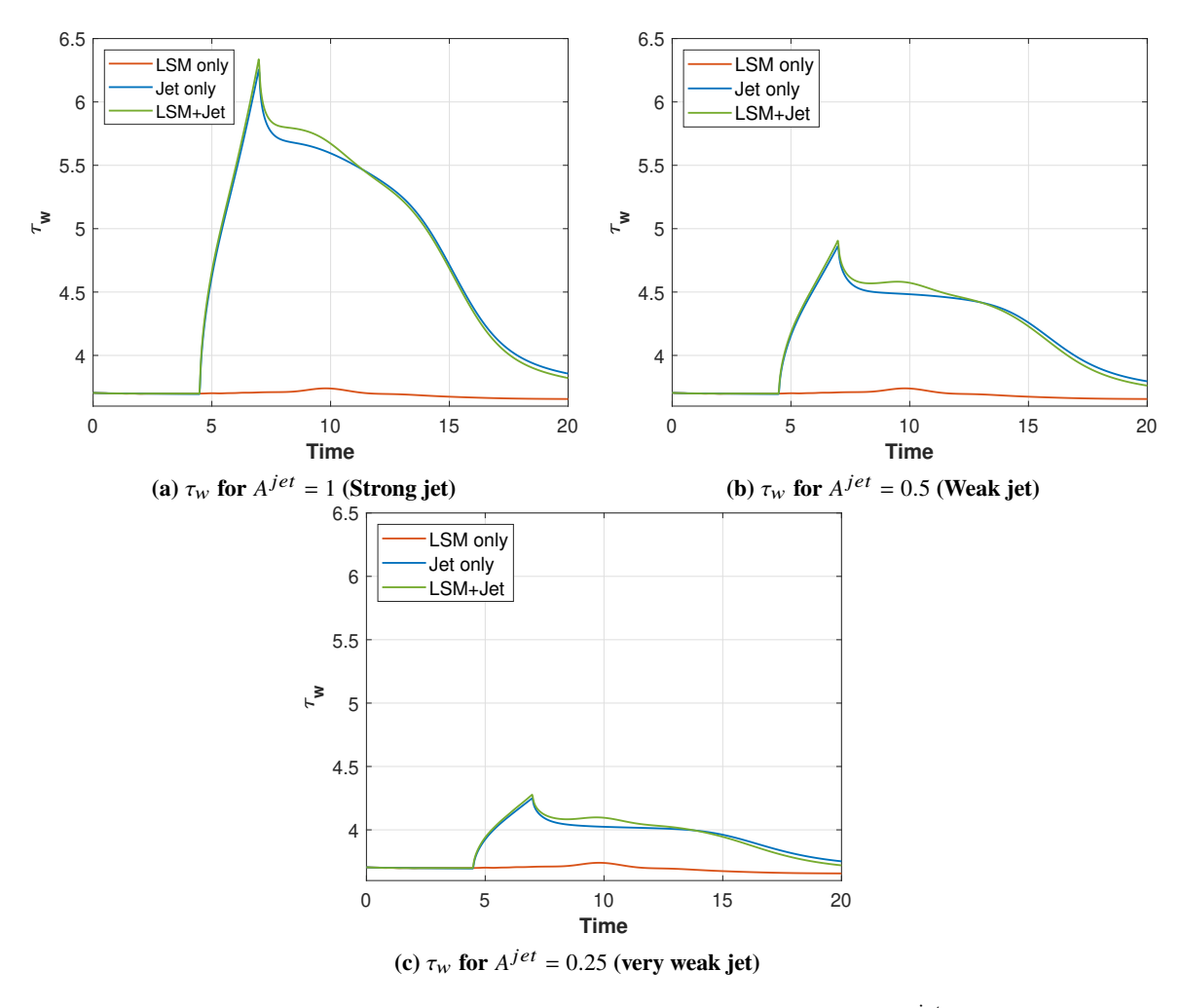


Fig. 8 Area-averaged wall shear stress plotted over time for 3 different values of A^{jet} – the scalar signal that controls the jet magnitude. For each value of the jet magnitude, three cases are compared: 1) only LSM without any jet actuation, 2) only jet without any LSM, and 3) LSM plus jet to capture the combined effect.

VI. Conclusion

Selectively manipulating the large-scale motions in a boundary layer for performance gains such as near-wall re-energization, drag reduction, mixing enhancement, and separation control can open many pathways for flow control. Toward that goal, we attempted to create synthetic LSMs in a laminar boundary layer and study the effect of targeting these synthetic turbulent structures and moving them toward the wall. After a study of the literature on LSMs, we created an external force field that can create a clean and stable series of hairpin vortices that resemble an LSM. The force field uses a tanh-smooth distribution located within the boundary layer and pushes the flow upstream, generating a low momentum zone. The parametric study presented shows how careful tuning of the parameters is necessary to find the optimal set of parameters for generating a clean packet of hairpin vortices at a given Reynolds number. Our choice of studying synthetic LSMs in a laminar boundary layer was motivated by the need to understand the effect of steering vortical structures in a simple, tractable setting before applying our strategy to steering naturally occurring LSMs in a turbulent boundary layer.

The generated synthetic LSMs were subsequently targeted by a downwash-inducing jet that pushed them toward the wall in order to enhance near-wall mixing. After a study of the wall shear stress and the distribution of the RMS vorticity fluctuation indicate that this actuation scheme – targeting LSMs with a jet – can lead to an increase in near-wall mixing compared to the effect that the LSMs and the jet have on the flow on their own. Subsequent work will test this control scheme with more principled control algorithms in a fully turbulent boundary layer setting.

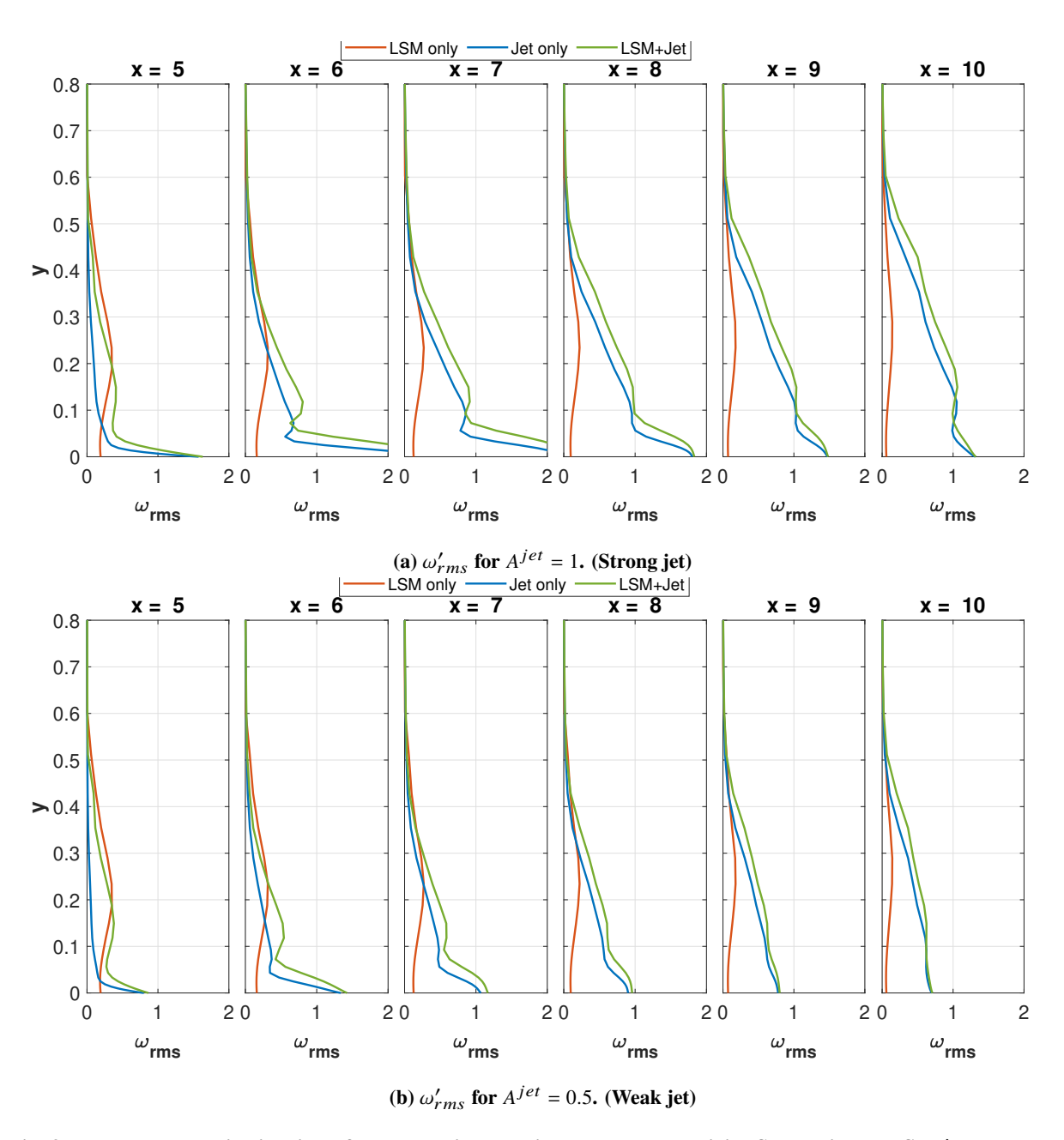


Fig. 9 Wall-normal distribution of the spanwise and time-averaged vorticity fluctuation RMS, ω'_{rms} , plotted at different streamwise locations immediately downstream of the actuator force field. a) $A^{jet}=1$. b) $A^{jet}=0.5$. For both jet magnitudes, we compare three cases: 1) LSM only case, 2) jet only case, and 3) LSM + jet.

VII. Acknowledgements

This work has been supported by the National Science Foundation awards 2129494 and 20528110. The authors acknowledge the Texas Advanced Computing Center (TACC) at the University of Texas at Austin for providing high-performance computing resources that have contributed to the results of this work. We would also like to thank Dr. Michael Amitay (Rensselaer Polytechnic Institute) and his group for their advice and discussions. The authors would also like to thank Pranav Sridhar for his help with reviewing the literature on large scale motions.

References

- [1] Liu, Z., Adrian, R. J., and Hanratty, T. J., "Large-scale modes of turbulent channel flow: transport and structure,", 2001.
- [2] Robinson, S. K., "Coherent motions in the turbulent boundary layer," Annu. Rev. Fluid Mech, Vol. 23, No. 1, 1991.
- [3] Brown, G. L., and Thomas, A. S. W., "Large structure in a turbulent boundary layer," *Citation: The Physics of Fluids*, Vol. 20, 1977, p. 243.
- [4] Falco, R. E., "Coherent motions in the outer region of turbulent boundary layers," *Citation: The Physics of Fluids*, Vol. 20, 1977, p. 124. doi:10.1063/1.861721.
- [5] Adrian, R. J., "Hairpin vortex organization in wall turbulence," *Physics of Fluids*, Vol. 19, No. 4, 2007, p. 41301.
- [6] Eitel-Amor, G., Örlü, R., Schlatter, P., and Flores, O., "Hairpin vortices in turbulent boundary layers," *Physics of Fluids*, Vol. 27, No. 2, 2015, p. 025108.
- [7] Kim, K., and Adrian, R., "Very large-scale motion in the outer layer," *Physics of Fluids*, Vol. 11, No. 2, 1999, pp. 417–422. Copyright: Copyright 2019 Elsevier B.V., All rights reserved.
- [8] Rahgozar, S., and Maciel, Y., "A visual assessment of hairpin packet structures in a DNS of a turbulent boundary layer," *European Journal of Mechanics B/Fluids*, Vol. 56, 2016, pp. 161–171.
- [9] Lee, J., Sung, H., and Adrian, R., "Space-time formation of very-large-scale motions in turbulent pipe flow," *Journal of Fluid Mechanics*, Vol. 881, 2019, pp. 1010–1047.
- [10] Lee, J., Lee, J. H., Choi, J.-I., and Sung, H. J., "Spatial organization of large- and very-large-scale motions in a turbulent channel flow," *Journal of Fluid Mechanics*, Vol. 749, 2014, p. 818–840.
- [11] Balakumar, B. J., and Adrian, R. J., "Large- and Very-Large-Scale Motions in Channel and Boundary-Layer Flows," *Philosophical Transactions: Mathematical, Physical and Engineering Sciences*, Vol. 365, No. 1852, 2007, pp. 665–681.
- [12] Matsuura, K., "Hairpin vortex generation around a straight vortex tube in a laminar boundary-layer flow,", 2018.
- [13] Paul F. Fischer, J. W. L., and Kerkemeier, S. G., "nek5000 Web page,", 2008. Http://nek5000.mcs.anl.gov.
- [14] Offermans, N., Marin, O., Schanen, M., Gong, J., Fischer, P., Schlatter, P., Obabko, A., Peplinski, A., Hutchinson, M., and Merzari, E., "On the strong scaling of the spectral element solver Nek5000 on petascale systems," *Proceedings of the Exascale Applications and Software Conference 2016*, 2016, pp. 1–10.
- [15] Hosseini, S. M., Vinuesa, R., Schlatter, P., Hanifi, A., and Henningson, D. S., "Direct numerical simulation of the flow around a wing section at moderate Reynolds number," *International Journal of Heat and Fluid Flow*, Vol. 61, 2016, pp. 117–128.
- [16] Brauner, T., Laizet, S., Benard, N., and Moreau, E., "Modelling of dielectric barrier discharge plasma actuators for direct numerical simulations," 8th AIAA Flow Control Conference, 2016, p. 3774.
- [17] Barros, J. M., and Christensen, K. T., "Characteristics of large-scale and superstructure motions in a turbulent boundary layer overlying complex roughness," *Journal of Turbulence*, Vol. 20, No. 2, 2019, pp. 147–173.
- [18] Tsolovikos, A., Suryanarayanan, S., Bakolas, E., and Goldstein, D., "Model Predictive Control of Material Volumes with Application to Vortical Structures," *AIAA Journal*, Vol. 59, No. 10, 2021, pp. 4057–4070.